Solid-State ^{199}Hg MAS NMR Studies of Mercury(II) Thiocyanate Complexes and Related Compounds. Crystal Structure of $Hg(SeCN)_2$

Graham A. Bowmaker,*,† Andrei V. Churakov,‡ Robin K. Harris,* Judith A. K. Howard, and David C. Apperley

Department of Chemistry, University of Durham, South Road, Durham DH1 3LE, United Kingdom

Received January 3, 1997

The solid-state ^{199}Hg MAS NMR spectra of $[Hg(SCN)_2]$, $[Hg(SeCN)_2]$, $M[Hg(SCN)_3]$, $M_2[Hg(SCN)_4]$ (M = K, Cs), and $K_2[Hg_3(NCO)_8]$ have been measured, and the (monoclinic) crystal structure of $[Hg(SeCN)_2]$ has been determined to assist in the interpretation of the NMR data. The asymmetric unit of $Hg(SeCN)_2$ contains one molecule at an inversion center which shows linear Se−Hg−Se bonding (Hg−Se = 2.4738(10) Å, Se−Hg−Se = 180°, Hg−Se−C = 97.5(3)°). Secondary Hg---Se and Hg---N contacts are 3.4246(9) and 2.835(12) Å, respectively; this arrangement differs from that in $Hg(SCN)_2$ where there are no secondary Hg---S contacts. A redetermination of the monoclinic crystal structure of $K[Hg(SCN)_3]$ is also reported, revealing substantial differences from the earlier work. Spinning sideband analysis has been used to determine the ^{199}Hg shielding anisotropy and asymmetry parameters $\Delta\sigma$ and η from the solid-state ^{199}Hg MAS NMR spectra. The effects of changes in the mercury coordination number and of distortion of the coordination environment on the shielding parameters are interpreted in terms of changes in the local paramagnetic contribution. The same method is employed to assess the effects of secondary bonding on shielding, and it is shown that the substantial differences between the values for $Hg(SCN)_2$ and $Hg(SeCN)_2$ can be attributed to these effects. The ν(HgS) modes have been assigned in the IR and Raman spectra of the thiocyanate complexes, and the correlation between the wavenumbers and splittings of these bands and the ^{199}Hg shielding parameters is discussed.

Introduction

With the recent developments which have taken place in high-resolution NMR techniques for solids,[1−10] there has been increasing interest in the solid-state NMR spectra of heavy-metal nuclei.[4,5] Until recently, there were very few solid-state NMR studies involving ^{199}Hg, but in the last few years there has been a considerable increase in the number of such investigations.[4,5,11−18] A significant number of these studies involve complexes with thiolate ligands,[11,14−17] the main interest in this group of compounds being the important role played by such ligands in the biological chemistry of the group 12 metals.[11,19−23] These studies have resulted in correlations between the ^{199}Hg solid-state NMR parameters and the structures of the complexes.[11,14,15,17] Such correlations are of potential value in the investigation of mercury coordination environments in situations where structural data are not readily obtainable by other methods.[11]

Most of the thiolate ligands involved in the studies carried out to date have rather complex structures, and it is somewhat surprising that few studies of the relationship between the ^{199}Hg solid-state NMR parameters and structure have been carried out using complexes with simpler ligands. Such studies should provide further tests of the validity of the correlations which have been established in the earlier work. Also, since the correlations which have been presented to date are essentially

† Permanent address: Department of Chemistry, University of Auckland, Private Bag 92019, Auckland, New Zealand.

‡ Permanent address: N. S. Kurnakov Institute of General and Inorganic Chemistry, Russian Academy of Science, 31 Leninskii prospekt, Moscow 117907, Russia.

(1) Haeberlen, U. *Adv. Magn. Reson., Suppl. 1* 1976.
(2) Fyfe, C. A. *Solid State NMR for Chemists;* C.F.C. Press: Guelph, Canada, 1983.
(3) Harris, R. K. *Nuclear Magnetic Resonance Spectroscopy;* Longman: Harlow, U.K., 1986.
(4) Davies, J. A.; Dutremez, S. *Coord. Chem. Rev.* **1992**, *114*, 201.
(5) Sebald, A. *NMR Basic Principl. Prog.* **1994**, *31*, 91.
(6) Harris, R. K.; Jackson, P.; Merwin, L. H.; Say, B. J.; Hägele, G. *J. Chem. Soc., Faraday Trans. 1* **1988**, *84*, 3649.
(7) Harris, R. K. *Chem. Brit.* **1993**, 601.
(8) Mehring, M. In *NMR Basic Principles and Progress;* Diehl, P., Fluck, E., Günther, H., Kosfeld, R., Eds.; Springer Verlag: Berlin, 1976; Vol. 11.
(9) Diehl, P., Fluck, E., Günther, H., Kosfeld, R., Seelig, J., Eds. *NMR Basic Principles and Progress;* Springer Verlag: Berlin, 1994; Vols. 30−33.
(10) Stejskal, E. O.; Memory, J. D. *High Resolution NMR in the Solid State;* Oxford University Press: Oxford, U.K., 1994.
(11) Wright, J. G.; Natan, M. J.; MacDonnell, F. M.; Ralston, D. M.; O'Halloran, T. V. *Prog. Inorg. Chem.* **1990**, *38*, 323.
(12) Harris, R. K.; Sebald, A. *Magn. Reson. Chem.* **1987**, *25*, 1058.
(13) Ambrosius, F.; Klaus, E.; Schaller, T.; Sebald, A. Z. *Naturforsch., A* **1995**, *50*, 423.
(14) Natan, M. J.; Millikan, C. F.; Wright, J. G.; O'Halloran, T. V. *J. Am. Chem. Soc.* **1990**, *112*, 3255.
(15) Santos, R. A.; Gruff, E. S.; Koch, S. A.; Harbison, G. S. *J. Am. Chem. Soc.* **1991**, *113*, 469.
(16) Han, M.; Peerson, O. B.; Bryson, J. W.; O'Halloran, T. V.; Smith, S. O. *Inorg. Chem.* **1995**, *34*, 1187.
(17) Bowmaker, G. A.; Dance, I. G.; Harris, R. K.; Henderson, W.; Laban, I.; Scudder, M. L.; Oh, S.-W. *J. Chem. Soc., Dalton Trans.* **1996**, 2381.
(18) Eichele, K.; Kroeker, S.; Wu, G.; Wasylishen, R. E. *Solid State NMR* **1995**, *4*, 295.
(19) Kägi, J. H. R., Kojima, Y., Eds. *Metallothionein II;* Birkhäuser: Basle, 1987.
(20) Furey, W. F.; Robbins, A. H.; Clancy, L. L.; Winge, D. R.; Wang, B. C.; Stout, C. D. *Science* **1986**, *231*, 704.
(21) Gruff, E. S.; Koch, S. A. *J. Am. Chem. Soc.* **1990**, *112*, 1245.
(22) Wright, J. G.; Tsang, H.-T.; Penner-Hahn, J. E.; O'Halloran, T. V. *J. Am. Chem. Soc.* **1990**, *112*, 2434.
(23) Watton, S. P.; Wright, J. G.; MacDonnell, F. M.; Bryson, J. W.; Sabat, M.; O'Halloran, T. V. *J. Am. Chem. Soc.* **1990**, *112*, 2824.

S0020-1669(97)00011-6 CCC: $15.00
Published on Web 03/20/1998

empirical in nature, it was considered desirable to try to establish a more quantitative relationship between the solid-state NMR and structural parameters and to use this to assist in the interpretation of the data obtained for mercury complexes involving a wider variety of structural types.

For our present investigations in this area, we have chosen to study a series of complexes of the thiocyanate ligand (SCN^-), which is closely related to the thiolate ligands (RS^-) that have hitherto been the main focus of attention in this area. The main differences between these two ligand types are their size ($RS^- > SCN^-$), their basicity ($RS^- > SCN^-$), and the fact that SCN^- can bind to metal ions through the N atom as well as (or instead of) through the S atom.[24]

In the present paper we describe the results of ^{199}Hg MAS NMR studies of $Hg(SCN)_2$, $M[Hg(SCN)_3]$, and $M_2[Hg(SCN)_4]$ (M = K, Cs). The crystal structures of most of these compounds are known, and they show that this series involves a range of mercury environments from two- to four-coordination.[25−28] We have also included complexes of selenocyanate ($SeCN^-$) and cyanate (OCN^-) ligands in this study. The structure of mercury(II) selenocyanate, $Hg(SeCN)_2$, has not yet been reported. Since its ^{199}Hg MAS NMR spectrum showed substantial differences from that of $Hg(SCN)_2$, its crystal structure was determined in the present work. The structure of mercury(II) cyanate is also unknown. In fact, rather surprisingly, this compound has not been fully characterized in the literature. One of the few homoleptic mercury(II) cyanate complexes which have been fully characterized is $K_2[Hg_3(NCO)_8]$.[29] The crystal structure of this compound shows that it contains essentially molecular $Hg(NCO)_2$ units, with Hg−N rather than Hg−O bonding. It was therefore included in the present study to allow a comparison to be made with the results for $Hg(SCN)_2$ and $Hg(SeCN)_2$. The only previous report of a solid-state NMR study of compounds of the type discussed above is one in which several salts of the complex $[Hg(SCN)_4]^{2-}$ with proton-containing cations were examined as potential ^{199}Hg CP MAS NMR setup samples.[18]

Experimental Section

Materials. Commercial samples of potassium thiocyanate KSCN, cesium carbonate $Cs_2(CO_3)$, potassium selenocyanate KSeCN, potassium cyanate KOCN, mercury(II) thiocyanate $Hg(SCN)_2$, mercury(II) acetate $Hg(OAc)_2$ (Aldrich), ammonium thiocyanate NH_4SCN (Koch-Light AR), and mercury(II) nitrate monohydrate $Hg(NO_3)_2{\cdot}H_2O$ (BDH AnalaR) were used without further purification.

Preparation of Compounds. Potassium Tris(thiocyanato)mercurate(II), K[Hg(SCN)$_3$]. KSCN (0.78 g, 8.0 mmol) and $Hg(SCN)_2$ (2.53 g, 8.0 mmol) were added to absolute ethanol (70 cm^3), and the mixture was heated to boiling. The colorless crystalline solid which was obtained upon cooling the mixture was collected, washed with absolute ethanol (15 cm^3), and air-dried. Yield: 2.47 g (75%). Anal. Calcd for $C_3HgKN_3S_3$: C, 8.70; H, 0.0; N, 10.15. Found: C, 8.7; H: 0.0; N, 10.0. The crude product was recrystallized once from hot methanol. Crystals for the X-ray structure determination were obtained during an attempt to grow crystals of $K_2[Hg(SCN)_4]$: KSCN (1.20 g, 12.3 mmol) and $Hg(SCN)_2$ (1.90 g, 6.0 mmol) were added to absolute ethanol (12 cm^3), and the mixture was stirred at 55 °C until all the solids had dissolved. The solution was slowly cooled to 10 °C and then to 0 °C to yield well-formed crystals of the product, which were collected and washed with ice-cold ethanol. Yield: 0.13 g. This product was shown by IR spectroscopy to be identical to $K[Hg(SCN)_3]$ prepared by the first method described above.

Dipotassium Tetrakis(thiocyanato)mercurate(II), K$_2$[Hg(SCN)$_4$]. KSCN (1.20 g, 12.3 mmol) and $Hg(SCN)_2$ (1.90 g, 6.0 mmol) were added to absolute ethanol (20 cm^3), and the mixture was boiled until the volume of solution was about 2 cm^3. The product which separated as a colorless solid upon addition of diethyl ether (13 cm^3) was collected, washed with a 3:1 diethyl ether/absolute ethanol mixture (20 cm^3) followed by diethyl ether (8 cm^3), and air-dried. Yield: 2.58 g (84%). Anal. Calcd for $C_4HgK_2N_4S_4$: C, 9.40; H, 0.0; N, 10.96. Found: C, 9.4; H: 0.0; N, 10.7.

Cesium Thiocyanate, CsSCN. Cesium carbonate (1.88 g, 5.77 mmol) and ammonium thiocyanate (0.88 g, 11.5 mmol) were dissolved in water (10 cm^3), and the resulting solution was evaporated to dryness in an oven at 105 °C. Yield of colorless solid: 2.2 g (100%). This was used in subsequent syntheses without further purification.

Cesium Tris(thiocyanato)mercurate(II), Cs[Hg(SCN)$_3$]. CsSCN (1.20 g, 6.3 mmol) and $Hg(SCN)_2$ (1.99 g, 6.3 mmol) were added to absolute ethanol (20 cm^3), and the mixture was heated to boiling. The colorless crystalline solid which was obtained upon cooling the mixture was collected, washed with absolute ethanol, and air-dried. Yield: 2.93 g (92%). The crude product was recrystallized once from hot methanol. Anal. Calcd for $C_3CsHgN_3S_3$: C, 7.10; H, 0.0; N, 8.28. Found: C, 7.1; H: 0.0; N, 8.1.

Dicesium Tetrakis(thiocyanato)mercurate(II), Cs$_2$[Hg(SCN)$_4$]. CsSCN (0.99 g, 5.2 mmol) and $Hg(SCN)_2$ (0.82 g, 2.6 mmol) were added to absolute ethanol (10 cm^3), and the mixture was heated to boiling. The colorless crystalline solid which was obtained upon cooling the mixture was collected, washed with absolute ethanol, and air-dried. Yield: 1.69 g (93%). Anal. Calcd for $C_4Cs_2HgN_4S_4$: C, 6.88; H, 0.0; N, 8.02. Found: C, 6.8; H: 0.0; N, 7.6.

Dipotassium Octakis(cyanato)trimercurate(II), K$_2$Hg$_3$(NCO)$_8$. This was prepared by a modification of the literature method.[29] To an ice-cold solution of mercury(II) acetate, $Hg(OAc)_2$ (3.19 g, 10 mmol), in water (40 cm^3) acidified with glacial acetic acid (0.5 cm^3) was added with rapid stirring a solution of KNCO (3.24 g, 40 mmol) in water (40 cm^3). The resulting colorless precipitate was collected and washed with a small amount of ice-cold water. Yield: 2.33 g (72%). Anal. Calcd for $C_8Hg_3K_2N_8O_8$: C, 9.46; H, 0.0; N, 11.03. Found: C, 9.4; H: 0.0; N, 10.8.

Mercury(II) Selenocyanate, Hg(SeCN)$_2$. To a solution of $Hg(NO_3)_2{\cdot}H_2O$ (1.71 g, 5 mmol) in water (20 cm^3) containing concentrated nitric acid (0.4 cm^3) was added with stirring a solution of KSeCN (1.34 g, 9.3 mmol) in water (12 cm^3). The resulting colorless precipitate was collected by vacuum filtration, washed with distilled water (30 cm^3), and air-dried. Yield: 1.67 g (88%) (IR: ν(CN) = 2143, 2132 (lit.[30] 2140, 2130), ν(CSe) = 538 (lit.[30] 541) cm^{-1}.) Crystals for the X-ray crystal structure determination were obtained by slow evaporation at room temperature of a solution obtained by dissolving the product (0.1 g) in warm acetonitrile (20 cm^3). Care was required to avoid overheating of the solution, which results in decomposition of the compound to give a black deposit.

X-ray Crystallography. Crystallographic data for $Hg(SeCN)_2$ and $K[Hg(SCN)_3]$ are summarized in Table 1. The crystals were mounted on the tip of glass fiber using perfluorinated oil. All measurements were made on a Siemens SMART CCD diffractometer with graphite-monochromatized Mo Kα radiation (λ = 0.710 73 Å) at 150.0(2) K. The data were collected using the ω scan technique and were corrected for Lorentz and polarization effects. Siemens SAINT software[31] was used for data reduction. Empirical absorption corrections based on measurements of equivalent reflections (SHELXTL-Plus)[32] were used.

(24) (a) Burmeister, J. L. In *The Chemistry and Biochemistry of Thiocyanic Acid and Its Derivatives;* Newman, A. A., Ed.; Academic Press: London, 1975; pp 68−130. (b) Vrieze, K.; van Koten, G. In *Comprehensive Coordination Chemistry;* Wilkinson, G., Ed.; Pergamon: Oxford, U.K., 1987; Vol. 2, p 189.
(25) Beauchamp, A. L.; Goutier, D. *Can. J. Chem.* **1972**, *50*, 977.
(26) Zhdanov, G. S.; Sanadze, V. V. *Zh. Fiz. Khim.* **1952**, *26*, 469.
(27) Zvonkova, Z. V. *Zh. Fiz. Khim.* **1952**, *26*, 1798.
(28) Thiele, G.; Bauer, R.; Messer, D. *Naturwissenschaften* **1974**, *61*, 215.
(29) Thiele, G.; Hilfrich, P. *Z. Naturforsch., B* **1978**, *33*, 597.
(30) Aynsley, E. E.; Greenwood, N. N.; Sprague, M. J. *J. Chem. Soc.* **1965**, 2395.
(31) *SAINT Version 4.050*; Siemens Analytical X-ray Instruments Inc.: Madison, WI, 1995.
(32) Sheldrick, G. M. *SHELXTL-Plus, Release 4.1*; Siemens Analytical X-ray Instruments Inc.: Madison, WI, 1991.

Table 1. Crystallographic Data

	$Hg(SeCN)_2$	$K[Hg(SCN)_3]$
empirical formula	$C_2HgN_2Se_2$	$C_3HgKN_3S_3$
fw	410.55	413.93
cryst size, mm	0.55 × 0.40 × 0.15	0.38 × 0.10 × 0.08
cryst system	monoclinic	monoclinic
space group	$P2_1/c$	$P2_1/n$
a, Å	6.1245(2)	11.9119(3)
b, Å	4.2277(2)	4.0201(1)
c, Å	11.6449(5)	18.7095(3)
β, deg	92.131(2)	91.852(1)
V, Å^3	301.31(2)	895.47(3)
Z	2	4
d_{calc}, g cm^{-3}	4.525	3.070
T, K	150.0(2)	150.0(2)
λ, Å	0.71073	0.71073
μ, cm^{-1}	374.91	182.87
$F(000)$	348	744
w$R(F^2)$[a]	0.134	0.046
goodness-of fit on F^2	1.112	1.027
$R(F)$[b]	0.056	0.022

[a] $wR(F^2) = [\sum[w(F_o^2 - F_c^2)^2]/\sum[w(F_o^2)^2]]^{1/2}$. [b] $R(F) = \sum||F_o| - |F_c||/\sum|F_o|$.

Table 2. Atomic Fractional Coordinates (×10^4) and Equivalent Isotropic Displacement Parameters (Å^2 × 10^3) for $Hg(SeCN)_2$ and $K[Hg(SCN)_3]$

atom	x	y	z	U_{eq}[a]
		$Hg(SeCN)_2$		
Hg	0	5000	5000	42(1)
Se	1599(2)	1569(2)	6533(1)	35(1)
C	4478(15)	2292(23)	6252(10)	34(2)
N	6309(19)	2652(30)	6126(10)	55(2)
		$K[Hg(SCN)_3]$		
Hg	6844(1)	2103(1)	5396(1)	11(1)
K	9046(1)	7107(2)	3101(1)	11(1)
S(1)	7266(1)	1569(3)	6663(1)	15(1)
C(1)	5997(4)	2481(9)	6984(2)	13(1)
N(1)	5142(4)	3039(9)	7235(2)	17(1)
S(2)	8193(1)	−2837(2)	4898(1)	9(1)
C(2)	9153(4)	−2420(9)	5563(2)	10(1)
N(2)	9819(3)	−2136(9)	6024(2)	18(1)
S(3)	5582(1)	2654(2)	4339(1)	11(1)
C(3)	6581(4)	2325(9)	3723(2)	10(1)
N(3)	7264(3)	2078(9)	3304(2)	14(1)

[a] The equivalent isotropic displacement parameter, U_{eq}, is defined as one-third of the trace of the orthogonalized $\mathbf{U}_{ij}$ tensor.

The structures were solved by direct methods (SHELXS-86)[33] and refined by full-matrix least squares on F^2 (SHELXL-93)[34] with anisotropic thermal parameters for all atoms. SHELXTL-Plus[32] software was used to prepare materials for publication. Data reduction was performed on a DEC Alpha Station, and then structure solution and refinement were made on a Silicon Graphics Irix Indigo workstation. Final atomic coordinates for $Hg(SeCN)_2$ and $K[Hg(SCN)_3]$ are given in Table 2, and the structures are shown in Figures 1 and 2, respectively.

Spectroscopy. Carbon-13, selenium-77, and mercury-199 magic-angle spinning spectra were obtained at 75.43, 57.27, and 53.65 MHz, respectively, using a Varian Unity Plus 300 spectrometer. A 7.0 mm o.d. silicon nitride rotor with Vespel end-caps was used for all spectra, with spin rates in the range 1.5−10 kHz. Although measurements were nominally made at ambient probe temperature (*ca.* 25 °C), it is likely that the fast spinning used for the ^{199}Hg spectra resulted in substantially elevated temperatures (*ca.* 45 °C).[35] The carbon-13 spectrum was recorded with direct polarization (sometimes referred to as single-pulse excitation). A recycle delay of 5 s was used, and 15 000 transients were collected. Selenium-77 spectra were recorded with direct polarization. A recycle delay of 3 s was used, and 20 000 transients were collected. Mercury-199 spectra were recorded with direct polarization (1 μs 12° pulses as judged via cross polarization for a sample of $[Hg(dmso)_6][O_3SCF_3]_2$). Centerband signals were located by varying the spinning rate. Recycle delays of 3 s with ca. 20 000 transients were required to get acceptable spectra. Spinning sideband intensities were analyzed to yield values of the shielding tensor components by an iterative computer program written in-house.[36] The fitting procedure used a minimum of five sidebands plus the centerband and was carried out for spinning rates in the range 8500−9800 Hz for all compounds except $M[Hg(SCN)_4]$ (M = K, Cs), where the rates used were 1660 and 6000 Hz, respectively. Accuracy was limited by the high noise levels and because the spectra required baseline correction. Errors in the shielding tensor parameters were calculated by a published method.[37] They are statistical in nature and may underestimate the true errors, which would also have systematic and experimental reproducibility contributions. Chemical shifts were referenced using replacement samples of adamantane (δ_C = 38.4 ppm for the CH_2 carbon on the tetramethylsilane scale), ammonium selenate (δ_{Se} = 1040 ppm on the dimethyl selenide scale, and $[Hg(dmso)_6][O_3SCF_3]_2$ (δ_{Hg} = −2313 ppm[38] on the dimethylmercury scale).

Infrared spectra were recorded with 4 cm^{-1} resolution at room temperature as KBr disks on a Digilab FTS-60 Fourier-transform infrared spectrometer employing an uncooled DTGS detector. Far-infrared spectra were recorded with 2 cm^{-1} resolution at room temperature as pressed polythene disks on a Digilab FTS-60 Fourier-transform infrared spectrometer employing an FTS-60V vacuum optical bench with a 6.25 μm mylar film beam splitter, a mercury lamp source, and a pyroelectric triglycine sulfate detector. Raman spectra were recorded at 4.5 cm^{-1} resolution using a Jobin-Yvon U1000 spectrometer equipped with a cooled photomultiplier (RCA C31034A) detector. The 488.0 nm exciting line from a Spectra-Physics model 2016 argon-ion laser was used.

Results and Discussion

Crystal Structures. The molecular structure and the arrangement of the molecules in crystalline $Hg(SeCN)_2$ are shown in Figure 1. Selected distances and angles are given in Table 3. The basic structural unit is the centrosymmetric $Hg(SeCN)_2$ molecule, which shows linear Se−Hg−Se bonding. The two selenocyanate ligands lie almost perpendicular to the Se−Hg−Se(A) direction. In the solid-state structural chemistry of mercury, it is frequently observed that there are weaker secondary interactions as well as the primary bonding interactions involving the nearest-neighbor atoms.[39−44] This is the case in the present compound, where the linear Se−Hg−Se(A) coordination is expanded to a distorted octahedral environment by weaker interactions of the mercury atom with the two Se atoms Se(C), Se(C′) and the two N atoms N(B), N(B′) in four neighboring molecules (Figure 1b). The existence of such interactions can be deduced by comparison of the interatomic distances involved with the appropriate sums of van der Waals

(33) Sheldrick, G. M. *Acta Crystallogr., Sect. A* **1990**, *46*, 467.
(34) Sheldrick, G. M. *SHELXL-93. Program for the Refinement of Crystal Structures*; University of Göttingen: Göttingen, Germany, 1993.
(35) Bjorholm, T.; Jakobsen, H. J. *J. Magn. Reson.* **1989**, *84*, 204.
(36) (a) Ascenso, J. R.; Bai, H.; Harris, R. K. Unpublished results. (b) Harris, R. K.; Merwin, L. H.; Hägele, G. *J. Chem. Soc., Faraday Trans. 1* **1989**, *85*, 1409.
(37) Olivieri, A. C. *J. Magn. Reson., Ser. A* **1996**, *123*, 207.
(38) Hook, J. M.; Dean, P. A. W.; van Gorkom, L. C. M. *Magn. Reson. Chem.* **1995**, *33*, 77.
(39) Brodersen, K.; Hummel, H.-U. *Comprehensive Coordination Chemistry;* Wilkinson, G., Ed.; Pergamon: Oxford, U.K., 1987; Vol. 5, p 1047.
(40) Levason, W.; McAuliffe, C. A. In *The Chemistry of Mercury;* McAuliffe, C. A., Ed.; McMillan: London, 1977; p 49.
(41) Canty, A. J.; Deacon, G. B. *Inorg. Chim. Acta* **1980**, *45*, L225.
(42) Wells, A. F. *Structural Inorganic Chemistry*, 5th ed.; Clarendon Press: Oxford, U.K., 1984; pp 1156−1169.
(43) Grdenić, D. *Q. Rev. Chem. Soc.* **1965**, *19*, 303.
(44) Dean, P. A. W. *Prog. Inorg. Chem.* **1978**, *24*, 109.

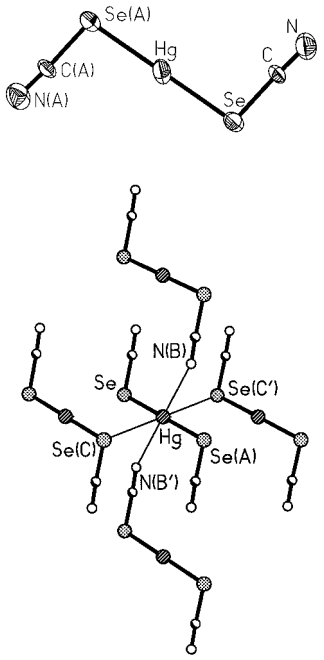

Figure 1. (a) Top: Molecular structure of $Hg(SeCN)_2$. Displacement ellipsoids are shown at 50% probability level. (b) Bottom: Part of the crystal lattice of $Hg(SeCN)_2$, showing the secondary bonding interactions.

Table 3. Selected Intramolecular and Intermolecular Distances and Angles in $Hg(SeCN)_2$[a]

	Distances (Å)		
Hg−Se	2.4738(10)	Hg−Se(C)	3.4246(9)
Se−C	1.831(9)	Hg−N(B)	2.835(12)
C−N	1.15(2)		
	Angles (deg)		
Se−Hg−Se(A)	180	Se−Hg−Se(C)	89.91(3)
Hg−Se−C	97.5(3)	Se−Hg−N(B)	76.2(2)
Se−C−N	176.4(10)		

[a] Symmetry transformations used to generate equivalent atoms: Se(A), $-x, 1-y, 1-z$; Se(C), $-x, -y, 1-z$; N(B), $1-x, 1-y, 1-z$.

radii. The effective nonbonding (van der Waals) shapes of several different main-group atoms in molecules in which these atoms are bound to a single carbon atom have been reported.[45] For N, the shape is virtually spherical, with a radius of 1.6 Å, whereas for Se the shape is spheroidal, with a smaller radius (1.7 Å) in the direction of the C−Se bond and a greater radius (2.15 Å) perpendicular to this bond. If the structure in Figure 1 is examined, it is clear that the latter radius is relevant for $Hg(SeCN)_2$. Using a value of 1.70 Å for Hg,[41,46] the appropriate sums are Hg,N = 3.30 and Hg,Se = 3.85 Å. Since these are greater than the observed Hg---N (2.835(12)) and Hg---Se (3.4246(9) Å) distances, the presence of secondary bonding interactions between these atoms is confirmed.

The structure of the $Hg(SeCN)_2$ molecule is very similar to that of $Hg(SCN)_2$.[25] Both involve linear coordination of the Hg atom by E = S or Se, and the Hg−E−C angles are equal within experimental error. The E−C−N angles deviate slightly from linearity in both cases. The main difference between the structures of these compounds concerns the secondary bonding. In both cases the primary E−Hg−E coordination is expanded to a distorted octahedral environment by the presence of weak

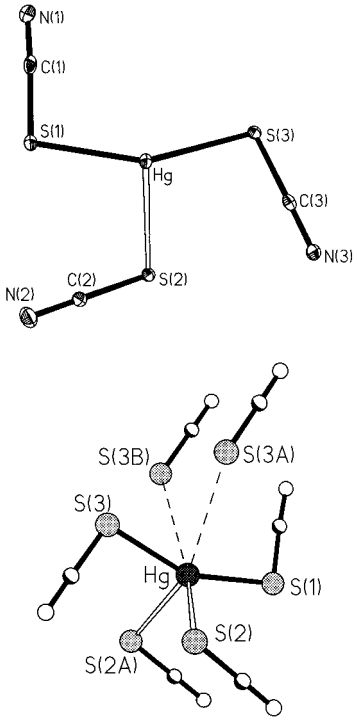

Figure 2. 2. (a) Top: Structure of "$[Hg(SCN)_3]^-$" in $K[Hg(SCN)_3]$. Displacement ellipsoids are shown at 50% probability level. (b) Bottom: Part of the crystal lattice of $K[Hg(SCN)_3]$, showing the secondary bonding interactions.

interactions between the mercury atom and atoms on four neighboring molecules. However, these interactions involve four Hg---N = 2.81 Å contacts in $Hg(SCN)_2$, compared with two Hg---N and two Hg---Se contacts in $Hg(SeCN)_2$ (see above). This difference has a significant effect on the ^{199}Hg MAS NMR spectra of these compounds (see below).

Attempts to grow single crystals of $K_2[Hg(SCN)_4]$ by slow crystallization from solutions containing KSCN and $Hg(SCN)_2$ in a 2:1 mole ratio yielded well-formed crystals of the 1:1 complex $K[Hg(SCN)_3]$ (see Experimental Section). Although the crystal structure of this compound has been reported previously,[26] doubts have been expressed about its correctness.[40] We have therefore redetermined this structure and have found significant differences from the previously published one, in respect of the space group, unit cell, and geometric parameters. The structure of the anion in $K[Hg(SCN)_3]$ is shown in Figure 2. Selected distances and angles are given in Table 4. The structure can be described as consisting of $Hg(SCN)_2$ molecules, Hg−S(1) = 2.4156(11), Hg−S(3) = 2.4553(11) Å, and S(l)−Hg−S(3) = 154.26(4)° (cf. solid $Hg(SCN)_2$: Hg−S = 2.381(6) Å, S−Hg−S = 180°),[25] which are significantly perturbed by secondary bonding interactions, Hg---S(2) = 2.7378(10), Hg---S(2A) = 2.7733(10) Å, and S(2)---Hg---S(2A) = 93.68(3)°. These secondary interactions involve "ionic" thiocyanates which do not take part in the strong primary bonding interactions described above. The two S atoms S(3A) and S(3B), which are involved in the longer of the two primary bonding interactions in two neighboring $Hg(SCN)_2$ molecules, lie at distances of 3.5133(11) and 3.6234(10) Å from the Hg atom and thus represent very weak or nonbonding interactions.

Solid-State NMR Spectra. The ^{199}Hg MAS NMR spectra of $Hg(SCN)_2$ and $Hg(SeCN)_2$ are shown in Figure 3. As with other mercury complexes which show large ^{199}Hg shielding anisotropy, the spectra consist of a centerband flanked by a number of spinning sidebands.[4,5,11−17] The spectra of $K_2[Hg-$

(45) Nyburg, S. C.; Faerman, C. H. *Acta Crystallogr., Sect. B* **1985**, *41*, 274.
(46) Bondi, A. *J. Phys. Chem.* **1966**, *70*, 3006.

Table 4. Selected Intramolecular and Intermolecular Distances and Angles in $K[Hg(SCN)_3]$[a]

	Distances (Å)		
Hg−S(1)	2.4156(11)	S(1)−C(1)	1.684(5)
Hg−S(3)	2.4553(11)	C(1)−N(1)	1.157(7)
Hg−S(2)	2.7378(10)	S(2)−C(2)	1.672(5)
Hg−S(2A)	2.7733(10)	C(2)−N(2)	1.159(6)
Hg−S(3A)	3.5133(11)	S(3)−C(3)	1.688(5)
Hg−S(3B)	3.6234(10)	C(3)−N(3)	1.152(6)
	Angles (deg)		
S(1)−Hg−S(3)	154.26(4)	C(1)−S(1)−Hg	99.8(2)
S(1)−Hg−S(2)	99.44(3)	N(1)−C(1)−S(l)	176.9(4)
S(1)−Hg−S(2A)	106.89(4)	C(2)−S(2)−Hg	93.9(2)
S(2)−Hg−S(2A)	93.68(3)	N(2)−C(2)−S(2)	179.9(4)
S(1)−Hg−S(3A)	87.67(3)	C(3)−S(3)−Hg	96.7(2)
S(1)−Hg−S(3B)	93.39(3)	N(3)−C(3)−S(3)	179.5(4)
S(3A)−Hg−S(3B)	68.55(2)		

[a] Symmetry transformations used to generate equivalent atoms: S(2A), N(3A), x, l + y, z; S(3A), 1 − x, −y, 1 − z; S(3B), 1 − x, 1 − y, 1 − z; N(1A), 0.5 + x, 0.5 − y, − 0.5 + z; N(1B), 0.5 + x, 1.5 − y, −0.5 + z; N(2A), 2 − x, −y, 1 − z; N(2B), 2 − x, 1 − y, 1 − z; N(3B), 1.5 − x, 0.5 + y, 0.5 − z.

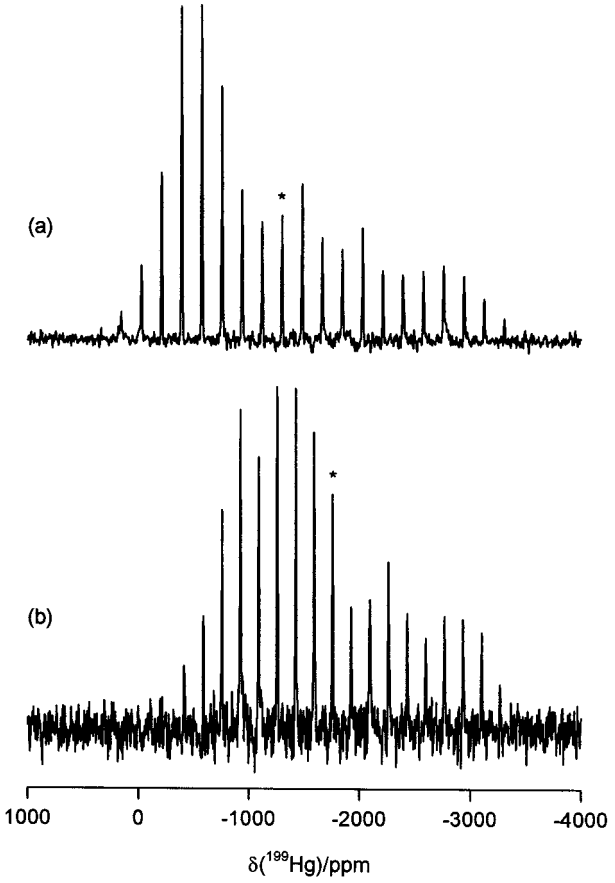

Figure 3. 53.6 MHz ^{199}Hg MAS NMR spectra of (a) $Hg(SCN)_2$ (spinning rate ν_s = 9780 Hz) and (b) $[Hg(SeCN)_2]$ (ν_s = 9000 Hz). Baseline corrections and line-broadening (500 Hz) have been applied prior to plotting. The centerband is indicated by an asterisk.

$(SCN)_4]$ and $Cs_2[Hg(SCN)_4]$, which show a lower degree of anisotropy, are shown in Figure 4. The chemical shift and shielding tensor parameters obtained from spinning sideband analyses of these, and of the other spectra obtained in this work, are compared with those of some related compounds in Table 5. The principal components σ_{11}, σ_{22}, and σ_{33} of the shielding

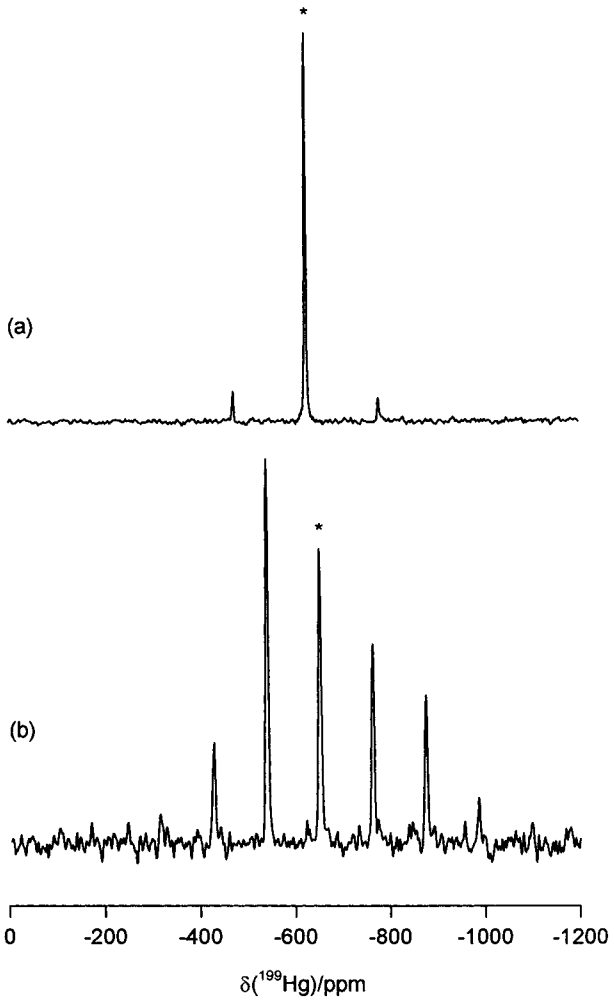

Figure 4. 53.6 MHz ^{199}Hg MAS NMR spectra of (a) $K_2[Hg(SCN)_4]$ (spinning rate ν_s = 8240 Hz) and (b) $Cs_2[Hg(SCN)_4]$ (ν_s = 6000 Hz). Baseline corrections and line-broadening (100 and 333 Hz, respectively) have been applied prior to plotting. The centerband is indicated by an asterisk.

tensor are defined such that

$$|\sigma_{33} - \sigma_{iso}| \geq |\sigma_{11} - \sigma_{iso}| \geq |\sigma_{22} - \sigma_{iso}| \quad (1)$$

where σ_{iso} is the isotropic, or scalar, shielding constant (relative to that of the bare nucleus), measured as

$$\sigma_{iso} - \sigma_{ref} = -\delta_{iso} \quad (2)$$

where δ_{iso} is the isotropic chemical shift (the centerband shift) and σ_{ref} is the shielding constant for the reference compound. Thus, σ_{iso} is related to the principal components of the shielding tensor by

$$\sigma_{iso} = (1/3)(\sigma_{11} + \sigma_{22} + \sigma_{33}) \quad (3)$$

The shielding anisotropy is defined as

$$\Delta\sigma = \sigma_{33} - {}^1/_2(\sigma_{11} + \sigma_{22}) \quad (4)$$

and the departure of the shielding tensor from axial symmetry is described by the asymmetry parameter

$$\eta = (\sigma_{22} - \sigma_{11})/(\sigma_{33} - \sigma_{iso}) \quad (5)$$

With the axis-labeling convention (eq 1), it can be shown that

(47) Bowmaker, G. A.; Churakov, A. V.; Harris, R. K.; Oh, S.-W. *J. Organomet. Chem.*, in press.

Table 5. ^{199}Hg Chemical Shifts and Shielding Tensor Parameters from Solid-State ^{199}Hg NMR Spectra

compd	$(\sigma_{11} - \sigma_{ref})$/ppm	$(\sigma_{22} - \sigma_{ref})$/ppm	$(\sigma_{33} - \sigma_{ref})$/ppm	δ_{iso}/ppm	$\Delta\sigma$/ppm	η	ref
$HgCl_2$	282(27)	573(26)	4019(26)	−1625	3592(37)	0.12(2)	47[a]
$Hg(SCN)_2$	81(23)	428(21)	3390(24)	−1300	3135(37)	0.17(2)	*b*
$Hg(SeCN)_2$	503(26)	1337(9)	3440(35)	−1760	2520(52)	0.50(1)	*b*
$[Hg(S\text{-}2,4,6\text{-}^iPr_3C_6H_2)_2]$	−627	−180	3852	−1015	4256	0.16	15
$[PPh_4][Hg(S\text{-}2,4,6\text{-}^iPr_3C_6H_2)_3]$	876	596	−672	−267	−1408	0.30	15
$[PPh_4][Hg(S\text{-}2,3,5,6\text{-}Me_4C_6H)_3]$[c]	1153	275	−685	−247	−1399	0.94	15
	1057	371	−601	−276	−1315	0.78	
$[N^nBu_4][Hg(SPh)_3]$	−494	326	1190	−341	1273	0.97	15
$[NMe_4][Hg(S^iPr)_3]$	433	433	−629	−79	−1062	0.00	16, 17
$K[Hg(SCN)_3]$	−49(15)	323(9)	1941(21)	−738	1805(32)	0.31(1)	*b*
$Cs[Hg(SCN)_3]$[d]	1623(21)	891(3)	−183(23)	−777	−1440(35)	0.76(1)	*b*
	1706(21)	879(1)	−43(21)	−847	−1335(32)	0.93(1)	
$K_2[Hg(SCN)_4]$	504.8(6)	580.6(2)	765.0(7)	−617	222(1)	0.51(1)	*b*
$Cs_2[Hg(SCN)_4]$	384.3(9)	572.3(3)	996(1)	−651	518(2)	0.54(1)	*b*
$[NH_4]_2[Hg(SCN)_4]$	355	655	1111	−707	606	0.74	18
$[NMe_4]_2[Hg(SCN)_4]$				−585			18
$[N\ ^nBu_4]_2[Hg(SCN)_4]$	695	695	454	−615	−241	0.00	18

[a] And references therein. [b] This work. [c] Two different crystalline phases. [d] Multiple signals due to site inequivalence.

$0 \leq \eta \leq 1$, with $\eta = 0$ corresponding to the case of axial symmetry ($\sigma_{11} = \sigma_{22}$). While η is always positive according to the above definitions, the anisotropy $\Delta\sigma$ may be either positive or negative, and this is reflected in the results in Table 5.

It has been suggested recently[48] that there are advantages to the use of alternative parameters to the anisotropy and asymmetry, namely the span, Ω, and skew, κ. For these, the principal axes of the shielding tensor are defined such that

$$\sigma_{11} \leq \sigma_{22} \leq \sigma_{33} \tag{6}$$

(contrast eq 1), while span and skew are defined as

$$\Omega = \sigma_{33} - \sigma_{11} \tag{7}$$

$$\kappa = 3(\sigma_{iso} - \sigma_{22})/(\sigma_{33} - \sigma_{11}) \tag{8}$$

However, nearly all the literature on shielding tensors has used $\Delta\sigma$ and η, so to keep the discussion simple we have continued to employ this convention here. We have listed all ^{199}Hg shielding tensor data using both conventions in a review article,[49] which seems to be the appropriate place to do so.

Empirical correlations between the anisotropic ^{199}Hg shielding parameters and the structures of mercury complexes, mostly dealing with complexes involving S-donor ligands, have been discussed in the past.[11,14−17] Thus, it has been found that the magnitude of the shielding anisotropy $\Delta\sigma$ decreases from linear MX_2 through trigonal planar MX_3 to tetrahedral MX_4 coordination, and the results of the present study provide further examples of this behavior. Thus $\Delta\sigma$ for $Hg(SCN)_2$ (3135 ppm), which shows linear HgS_2 coordination,[25] is much greater than that for $K_2[Hg(SCN)_4]$ (222 ppm), which involves tetrahedral MS_4 coordination.[27] However, the explanation of other aspects of the results, such as the decrease in $\Delta\sigma$ and the increase in η from $Hg(SCN)_2$ to $Hg(SeCN)_2$ and the change in the sign of $\Delta\sigma$ from $K_2[Hg(SCN)_3]$ to $Cs_2[Hg(SCN)_3]$, requires a more quantitative approach.

Anisotropic ^{199}Hg shielding parameters are amenable to interpretation on the basis of expressions that have been derived for the local paramagnetic contribution to the shielding.[49] Within the average excitation energy (AEE) approximation, the equations for the principal components of the local paramagnetic shielding tensor for the case where the shielding is due to electron density in the valence p orbitals only and the local symmetry is sufficiently high that cross terms in the charge density matrix are zero are

$$\sigma_{xx} = (n_y + n_z - n_y n_z)\,\sigma_p \tag{9}$$

$$\sigma_{yy} = (n_x + n_z - n_x n_z)\,\sigma_p \tag{10}$$

$$\sigma_{zz} = (n_x + n_y - n_x n_y)\,\sigma_p \tag{11}$$

where n_x, n_y, and n_z are the populations of the Hg $6p_x$, $6p_y$, and $6p_z$ orbitals, respectively (these populations can take values in the range 0−2), and

$$\sigma_p = -\mu_0 e^2 \hbar^2 \langle r^{-3} \rangle_{np} / 4\pi m^2 \Delta E \tag{12}$$

where μ_0 is the permeability constant, e is the electronic charge, m is the electron rest mass, and $\langle r^{-3} \rangle_{np}$ is the expectation value of r^{-3} for the valence np electron.[50,51] The average, or isotropic, local paramagnetic shielding derived from the above is

$$\sigma_{iso} = (1/3)[2n_x + 2n_y + 2n_z - n_x n_y - n_y n_z - n_x n_z]\sigma_p \tag{13}$$

Early applications of this model to the interpretation of isotropic ^{199}Hg shielding data showed some promise,[52] but the extreme scarcity of experimental data on ^{199}Hg anisotropic shielding and the limited understanding of the electronic structure of the complexes concerned prevented its wider application at that stage. We have shown that this approach allows a coherent interpretation of the anisotropic ^{199}Hg shielding data for a range of mercury compounds that have been studied more recently.[49] The most severe approximation involved in these equations is the average excitation energy approximation and the assumption that the average excitation energy ΔE does not vary much between the complexes concerned. In this work we consider complexes in which the S-donor ligands are chemically quite similar, and we assume that the ΔE values are correspondingly similar. Further work is required to establish whether this is the case. The alternative approach is to investigate the shielding parameters via ab initio

(48) Mason, J. *Solid State NMR* **1993**, *2*, 285.
(49) Bowmaker, G. A.; Harris, R. K.; Oh, S-W. *Coord. Chem. Rev.* **1997**, *167*, 49.
(50) Webb, G. A. In *NMR of Newly Accessible Nuclei;* Laszlo, P., Ed.; Academic Press: New York, 1983; Vol. 1, p 79.
(51) Jameson, C. J.; Gutowsky, H. S. *J. Chem. Phys.* **1964**, *40*, 1714.
(52) Harris, R. K., Mann, B. E., Eds. *NMR and the Periodic Table;* Academic Press: London, 1978.

calculations, but this is a difficult computational task at present. Some progress in this area has been made,[53] but no calculations of anisotropic shielding parameters obtained in this way have been reported to date.

For linear two-coordinate compounds HgX_2 involving the σ-donor (non-π-donor) ligand X, the bonding is influenced by electron donation from the σ-donor orbital of X (or X^- if HgX_2 is a neutral complex) into the Hg $6p_z$ orbital (the *z* axis lying along the Hg−X bond direction), and the only nonzero population required for (9)−(11) is that of the $6p_z$ orbital, n_z. This yields $\sigma_{xx} = \sigma_{yy} = n_z\sigma_p$ and $\sigma_{zz} = 0$ (as expected for a linear molecule). Since σ_p is negative (eq 12), this yields $\sigma_{zz} > \sigma_{xx} = \sigma_{yy}$. If it is assumed that the diamagnetic contributions to the shielding are isotropic, and so contribute equally to all three principal components of the shielding tensor, the above relationship should also hold for the total shielding constant. Defining the principal axes of the shielding tensor according to (1) yields $\sigma_{33} > \sigma_{11} = \sigma_{22}$. Inspection of the results for HgX_2 species such as $HgCl_2$ and $Hg(SCN)_2$ in Table 5 shows that the experimental results correspond closely to this relationship, the small deviations from equality of σ_{11} and σ_{22} being due to slight departures from axial symmetry in the solid state. The shielding anisotropy $\Delta\sigma$ (eq 4) for linear HgX_2 is given by $\Delta\sigma = -n_z\sigma_p$. Since σ_p is negative, $\Delta\sigma$ is positive. Thus, $\Delta\sigma$ is proportional to the $6p_z$ population n_z which, in turn, is proportional to the σ-donor strength of the ligand. Therefore, a strong σ-donor ligand, such as a thiolate (RS^-), will result in a greater n_z than will a weaker σ-donor, such as Cl^-, and so $\Delta\sigma$ is predicted to be greater for $Hg(SR)_2$ than for $HgCl_2$. One $Hg(SR)_2$ complex which has a linear HgS_2 coordination geometry is [Hg(S-2,4,6-^{i}Pr$_3$C$_6$H$_2$)$_2$], and $\Delta\sigma$ for this compound is considerably greater than that for $HgCl_2$ (Table 5). This is a direct reflection of the greater basicity of the thiolate ligand relative to Cl^-. The $\Delta\sigma$ values for $HgCl_2$ and $Hg(SCN)_2$ are more nearly equal, reflecting the similarity in the base strengths of the halide (Cl^-) and pseudohalide (SCN^-) ligands. A more detailed comparison is complicated by the fact that the observed difference between the $\Delta\sigma$ values for these two compounds may also be partly due to differences in secondary bonding interactions, as will be discussed below.

The type of analysis described above for linear HgX_2 species can also be applied to planar three-coordinate HgX_3 compounds. For the case in which all three Hg−X bonds are symmetrically equivalent, the Hg 6p orbital populations are $n_x = n_y$ and $n_z = 0$ (the *x*, *y* axes lie in the HgX_3 plane; *z* is perpendicular to this plane). Substitution into (9)−(11) yields $\sigma_{xx} = \sigma_{yy} = n_x\sigma_p$ and $\sigma_{zz} = (2n_x - n_x^2)\sigma_p$. The shielding anisotropy is thus $\Delta\sigma = n_x(1 - n_x)\sigma_p$. Unlike the linear two-coordinate case, for which $\Delta\sigma$ is always positive, $\Delta\sigma$ for the trigonal planar case may be positive or negative depending on whether n_x ($=n_y$) is greater or less than 1. The only complex having a perfectly trigonal planar mercury environment for which shielding anisotropy data are available is $[Hg(S^iPr)_3]^-$ (Table 5).[16,17] For this complex, $\Delta\sigma$ is negative, implying that n_x ($=n_y$) < 1. This is chemically reasonable; for pure covalent metal−ligand bonding involving sp^2 hybrid orbitals on mercury, $n_x = n_y = 1$, but these populations are expected to be less than this limiting value because (a) the degree of ligand-to-metal charge transfer will generally be less than that required for a pure covalent bond and (b) the Hg 6s orbital is lower in energy than the Hg 6p orbitals, so that more electron density will reside in the s orbital than in the p orbitals, compared with the values predicted on the basis of ideal sp^2 hybridization. This is supported by the results of recent calculations.[54] There is thus a distinct and diagnostic difference between the shielding anisotropies for linear and trigonal coordination; $\Delta\sigma$ should normally be positive for the linear HgX_2 geometry and negative for the trigonal planar HgX_3 geometry, in good agreement with the experimental observations.

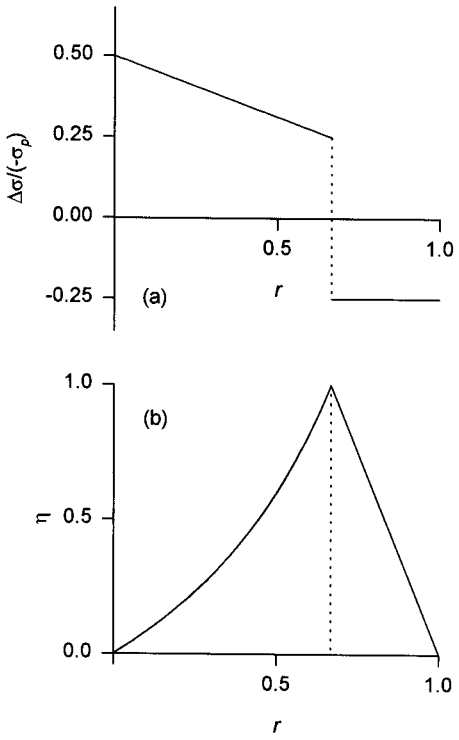

Figure 5. Dependence of (a) $\Delta\sigma$ and (b) η on *r* for the transition from linear HgX_2 ($r = 0$) to trigonal planar HgX_3 ($r = 1$) coordination for the case $n = 0.5$. (For details, see the text.)

Exact trigonal planar HgX_3 coordination is rare, and $[Hg(S^iPr)_3]^-$ is the only case for which ^{199}Hg shielding anisotropy data are available. There are, however, several examples of distorted trigonal planar coordination in which one of the X ligands is more weakly bonded than the other two. In order to investigate the consequences of such a distortion on the shielding parameters, calculations based on a simple model have been carried out. In this model the HgX_3 unit lies in the *xy* plane, with one of the HgX bonds lying along the *y* axis. The populations of the Hg $6p_x$ and $6p_y$ orbitals in the symmetrical HgX_3 case are equal and are set equal to *n*. A distortion involving the weakening of the Hg−X bond along the *y* direction is represented by a reduction in the population of the $6p_y$ orbital by a factor *r*, so that the population of this orbital is *rn*. Substitution of the populations into (9)−(11) yields $\sigma_{xx} = rn\sigma_p$, $\sigma_{yy} = n\sigma_p$, and $\sigma_{zz} = n(1 + r - rn)\sigma_p$. According to the definition (1), $\sigma_{11} = \sigma_{xx}$, $\sigma_{22} = \sigma_{yy}$, and $\sigma_{33} = \sigma_{zz}$ for $r > 1/(2 - n)$ and $\sigma_{11} = \sigma_{zz}$, $\sigma_{22} = \sigma_{yy}$, and $\sigma_{33} = \sigma_{xx}$ for $r < 1/(2 - n)$. The dependence of $\Delta\sigma$ and η on *r* calculated from eqs 4 and 5 for the case $n = 0.5$ is shown in Figure 5. The region near $r = 1$ corresponds to a small distortion of trigonal HgX_3 toward a C_{2v} X_2Hg---X structure; a decrease in *r* corresponds to an increase in the degree of distortion. The results in Figure 5 show that $\Delta\sigma$ is quite insensitive to this distortion, whereas η is strongly affected by it. This appears to correspond well with experimental observations for distorted three-coordinate com-

(53) Nakatsuji, H.; Hada, M.; Kaneko, H.; Ballard, C. C. *Chem. Phys. Lett.* **1996**, *255*, 195.

(54) Åkesson, R.; Persson, I.; Sandström, M.; Wahlgren, U. *Inorg. Chem.* **1994**, *33*, 3715.

pounds. Thus, for example, the complex $[Hg(S\text{-}2,3,5,6\text{-}Me_4C_6H)_3]^-$, which contains an HgS_3 coordination environment which is distorted in the sense described above,[15] yields $\Delta\sigma \approx -1400$ ppm and $\eta \approx 0.9$ (Table 5). By contrast, the closely related complex $[Hg(S\text{-}2,4,6\text{-}{}^i Pr_3C_6H_2)_3]^-$, which has almost perfect trigonal planar HgS_3 coordination,[15] also yields $\Delta\sigma \approx -1400$ ppm but gives a considerably lower asymmetry parameter $\eta \approx 0.3$ (Table 5). Thus, the prediction from Figure 5 that η is a much more sensitive indicator of distortion from trigonal planar coordination than $\Delta\sigma$ appears to be borne out by experiment. Figure 5 also predicts that beyond a certain point in the distortion ($r = {}^2/_3$ in this example) the sign of $\Delta\sigma$ switches from negative to positive, while η remains close to 1. The significance of such a sign change should not be overemphasized, since in some senses it is merely an artifact resulting from the convention of eqs 4 and 5. On the other hand, it occurs at the situation where σ_{22} is midway between σ_{11} and σ_{33}. Moreover, the sign is a measurable quantity. Such a sign change appears to occur in the case of the complex $[Hg(SPh)_3]^-$, which shows a slightly greater degree of distortion than that in $[Hg(S\text{-}2,3,5,6\text{-}Me_4C_6H)_3]^-$ [15] and which yields $\Delta\sigma \approx 1274$ ppm and $\eta \approx 0.97$ (Table 5).

An alternative way of describing the anisotropic ^{199}Hg shielding parameters is via the span and skew (eqs 7 and 8). The cases of linear and ideal trigonal coordination both involve axial symmetry ($\eta = 0$), and these yield $\Omega = |\Delta\sigma|$ and $\kappa = +1$ (linear) or $\kappa = -1$ (trigonal). For the situation described in Figure 5, Ω changes continuously from $-0.5\sigma_p$ for linear coordination to $-0.25\sigma_p$ for trigonal coordination, while κ changes continuously from $+1$ for linear coordination to -1 for trigonal coordination. The change in the sign of κ occurs under exactly the same conditions as the change in sign of $\Delta\sigma$. Plots similar to Figure 5 can be derived for Ω and κ.[49]

Linear two-coordinate complexes HgX_2 often show secondary bonding interactions to ligands which lie perpendicular to the X−Hg−X axis (the *z* axis). For the case of an interaction with a single ligand Y which lies on a 2-fold axis passing through the Hg atom (the *y* axis), the $6p_z$ orbital has a population *n* due to bonding with the two X ligands and the $6p_y$ orbital has a small population due to bonding with the Y ligand. If the $6p_y$ population is set equal to *rn*, then this situation corresponds to the one already discussed above for the strongly distorted trigonal coordination case. The isolated linear HgX_2 case corresponds to $r = 0$, and this results in a large positive $\Delta\sigma$ and $\eta = 0$ as expected (Figure 5). For weak interactions with the third ligand Y, $r \ll 1$, and this results in a decrease in $\Delta\sigma$ and an increase in η (Figure 5). Note the contrast with the case of distortion of HgX_3 from D_{3h} symmetry ($r \approx 1$), where $\Delta\sigma$ is quite insensitive to the degree of distortion. The analysis for the case of a linear HgX_2 unit involved in secondary bonding to two ligands Y which lie on the *y* axis and on opposite sides of the Hg atom is essentially the same as the case just discussed, and solid $Hg(SeCN)_2$ may be considered as an example of this situation. The primary bonding involves two strong, collinear Hg−Se bonds, but there are two secondary Hg---Se interactions perpendicular to the main Se−Hg−Se unit (see above). This results in $\Delta\sigma = 2520$ ppm and $\eta = 0.50$ (Table 5). This can be compared with the case of $Hg(SCN)_2$, in which there are no secondary Hg---S interactions (see above) and which yields $\Delta\sigma = 3136$ ppm and $\eta = 0.17$ (Table 2). In both cases there are Hg---N interactions perpendicular to the Se−Hg−Se or S−Hg−S direction (see above). The larger η value for $Hg(SeCN)_2$ implies that the Hg---N and Hg---Se interactions are of unequal strength, in that they result in unequal populations of the Hg $6p_x$ and $6p_y$ orbitals. The following experimental observations are consistent with the view that the Hg---Se interaction is the stronger one. The Hg---N bonding in $Hg(SeCN)_2$ is not very different from that in $Hg(SCN)_2$ (Hg---N = 2.84, 2.81 Å, respectively; see above). If the Hg---Se bonding in $Hg(SeCN)_2$ were weaker than the Hg---N bonding, then the net secondary bonding in this compound would be less than that in $Hg(SCN)_2$, so that $\Delta\sigma$ should be greater in $Hg(SeCN)_2$. The experimental results (Table 5) show that the opposite is the case, so it is concluded that the smaller $\Delta\sigma$ and the larger η values in $Hg(SeCN)_2$ are due mainly to the secondary Hg---Se bonding.

The very different $\Delta\sigma$ and η values observed for $K[Hg(SCN)_3]$ compared with $Cs[Hg(SCN)_3]$ (Table 5) are the consequence of structural differences between these compounds and can be understood in terms of the analyses discussed above. $K[Hg(SCN)_3]$ contains $Hg(SCN)_2$ molecules with two secondary Hg---S interactions. This is therefore similar to the case of $Hg(SeCN)_2$ discussed above, the main difference being that these interactions are approximately perpendicular to each other in $K[Hg(SCN)_3]$ (Table 4). The effect of these secondary Hg---S interactions is to reduce $\Delta\sigma$, and this is evident in the considerably lower value of this parameter for $K[Hg(SCN)_3]$ relative to that for $Hg(SCN)_2$ (Table 5). However, the value is still relatively large and has a positive sign, consistent with the presence of the approximately linear $Hg(SCN)_2$ molecule as the primary structural unit in this complex. By contrast, the compound $Cs[Hg(SCN)_3]$ contains units which are better described as distorted $[Hg(SCN)_3]^-$ ions. There are two such ions in the asymmetric unit (Hg(1)−S = 2.44, 2.45, 2.56 Å; S−Hg(1)−S = 132.3, 108.9, 116.3°; Hg(2)−S = 2.43, 2.48, 2.57 Å; S−Hg(2)−S = 129.2, 106.6, 124.0°).[28] In agreement with the crystal structure, two signals and associated sidebands are observed in the ^{199}Hg MAS NMR spectrum. The shielding parameters for the two sites are quite similar (Table 5), consistent with the similar coordination environments observed for these sites. In both cases, the shielding anisotropy $\Delta\sigma$ is negative, which is typical of three-coordinate HgS_3 coordination (see above). The asymmetry parameter η is large for both sites, reflecting the significant distortion from perfect trigonal planar coordination. In fact the distortion is essentially of the type involved in the model used to calculate the results in Figure 5; one of the Hg−S bonds is significantly longer than the other two, and the large η values suggest that this distortion is almost large enough to cause a reversal in the sign of $\Delta\sigma$. However, the relative independence of $\Delta\sigma$ from the degree of distortion (see discussion above and Figure 5) permits the conclusion that $\Delta\sigma$ for ideal trigonally coordinated $[Hg(SCN)_3]^-$ should be approximately -1400 ppm. The magnitude of this quantity is not much less than half of that for $Hg(SCN)_2$, in agreement with the predicted relative magnitudes for ideal HgS_2 ($r = 0$) and HgS_3 ($r = 1$) environments in Figure 5.

The case of ideal tetrahedral HgX_4 coordination is a particularly simple one; the populations n_x, n_y, and n_z are all equal in this case, and (9)−(11) show that all three principal components of the shielding tensor should be the same, so that $\Delta\sigma = 0$, as expected on the basis of symmetry. The only cases reported to date which show no detectable departure from isotropic ^{199}Hg shielding in the solid state are $[Hg(CN)_4]^{2-}$ complexes in which the Hg atoms occupy crystallographic sites of cubic symmetry.[18,55] However, $\Delta\sigma$ values for several compounds containing the $[Hg(SCN)_4]^{2-}$ complex lie in the range -241 to 606 ppm (Table 5). The nonzero $\Delta\sigma$ values must arise from distortions of the HgS_4 environment from ideal tetrahedral geometry. In fact, ideal T_d symmetry is not

(55) Wu, G.; Wasylishen, R. E. *J. Phys. Chem.* **1993**, *97*, 7863.

compatible with the nonlinear Hg−S−C geometry which occurs in these complexes, but the low value of $\Delta\sigma$ found for $K_2[Hg(SCN)_4]$ shows that this is not the primary cause of the relatively large $\Delta\sigma$ values in the other $[Hg(SCN)_4]^{2-}$ compounds. It appears that $\Delta\sigma$ and η are determined primarily by the arrangement of the atoms directly bonded to the Hg atom and that the arrangement of the other atoms in the ligands play a relatively minor role. The η values vary over the range 0−0.74, and there is no simple relationship between the $\Delta\sigma$ and η values. This is not unexpected, since a variety of different kinds of distortion from the ideal tetrahedral HgS_4 environment are possible, and no attempt has yet been made to correlate these with the shielding anisotropy and asymmetry parameters.

Isotropic shielding constants σ_{iso} are obtained directly from the centerband shifts δ_{iso}, which are listed in Table 5. The relationship of this parameter to the electronic structure of the complex is given in (13). The main structure types and associated 6p orbital populations normally encountered in mercury complexes are as follows: linear HgX_2 ($n_x = n_y = 0$; $n_z = n$); trigonal planar HgX_3 ($n_x = n_y = n$; $n_z = 0$); tetrahedral HgX_4 ($n_x = n_y = n_z = n$). Substitution into (13) yields the following relationships for $0 < n < 1$: $\sigma_{iso}(HgX_2) \gg \sigma_{iso}(HgX_3) > \sigma_{iso}(HgX_4)$, with the latter two becoming equal for populations $n = 1$. The prediction that linear HgX_2 complexes will show the greatest isotropic shielding is well borne out by the results in Table 5, but the situation is less clear-cut for HgX_3 and HgX_4 coordination. The greater sensitivity of the anisotropic parameters $\Delta\sigma$ and η to coordination geometry, compared with the isotropic parameter σ_{iso}, is particularly evident for the compounds $M[Hg(SCN)_3]$ (M = K, Cs). The σ_{iso} values are very similar and do not reflect the basic structural differences between these two compounds, which are clearly evident in the $\Delta\sigma$ and η values (see above).

The line widths in the ^{199}Hg MAS NMR spectrum of $K_2[Hg_3(NCO)_8]$ were very broad ($\Delta\nu_{1/2} = 2.6$ kHz, compared with 0.8 kHz for $Hg(SCN)_2$), which resulted in a S/N ratio which was too low to permit a spinning sideband analysis. However, $\sigma_{iso} = 1450$ ppm was measured from the centerband shift. This large value is consistent with the presence of essentially isolated $Hg(NCO)_2$ molecules with linear N−Hg−N bonding, as found in the crystal structure of this compound.[29] There are two molecules in the asymmetric unit in this structure, but the ^{199}Hg NMR lines were too broad to permit resolution of the expected two sets of signals. The ^{13}C MAS NMR spectrum consisted of a single broad line ($\delta = 137$ ppm, $\Delta\nu_{1/2} = 220$ Hz), despite the presence of ionic and Hg-bound cyanate ions in the structure. The reason for the unusually broad lines in the spectrum of this complex is not known at present, although a possible cause could be a transferred second-order quadrupolar effect of ^{14}N, as has been observed in ^{13}C MAS NMR spectra of cyanides.[55,56] In principle, (^{13}C, ^{14}N) isotropic indirect coupling could also cause line broadening, but this is not expected to be significant in the solid-state situation and has not been found in other cases.[56] The vibrational spectra display the features expected for the structure concerned (see below).

The ^{77}Se MAS NMR spectrum of $Hg(SeCN)_2$ shows a single line at 86.8 ppm, with ^{199}Hg satellites at a separation of $|^1J(^{199}Hg^{77}Se)| = 965$ Hz. It would be difficult to measure these parameters in solution, due to the low solubility of this compound and its instability in solution (see Experimental Section). While the $^1J(^{199}Hg^{77}Se)$ coupling is clearly resolved in the ^{77}Se MAS NMR spectrum, it is not visible at all in the corresponding ^{199}Hg spectrum, due to the greater line widths in the latter. The observation of a single ^{77}Se signal is consistent with the centrosymmetric structure found for this molecule in the crystal structure (see above). The only other compound containing Hg−Se bonds for which ^{77}Se MAS NMR spectra have been reported is $[Me_4N]_2[Hg(Se_4)_2]$, in which the Hg atom is tetrahedrally coordinated by two chelating tetraselenide (Se_4^{2-}) ligands; in this complex, $|^1J(^{199}Hg^{77}Se)| = 1220-1480$ Hz.[57]

Vibrational Spectra. It is of interest to compare how the structural properties of the solids studied in this work manifest themselves in their vibrational and NMR spectra. The IR spectrum of $Hg(SeCN)_2$ has been reported previously, and the bands assigned to the ν(CN) and ν(HgSe) modes both occur as doublets.[30] The reason for this is clear from the crystal structure: The two $Hg(SeCN)_2$ molecules in the unit cell lie on sites of C_i symmetry, and the factor group for the cell is C_{2h}. The IR-active (antisymmetric) ν(CN) and ν(HgSe) modes in the individual molecules have A_u symmetry under C_i, and this correlates with modes of $A_u + B_u$ symmetry (both IR active) under C_{2h}. Thus, the doubling of the IR bands is a factor-group splitting. This illustrates a general difference between the vibrational and NMR spectra. Both the site and factor groups are important in vibrational spectroscopy, and the existence of factor-group splittings which arise through coupling of the vibrations of molecules when there is more than one molecule in the unit cell complicates the interpretation of the spectra. The NMR spectrum, however, depends only on the site group and the number of atoms in the asymmetric unit. Thus, the single signals observed in the ^{199}Hg and ^{77}Se NMR spectra are consistent with the presence of one molecule in the asymmetric unit, with site symmetry C_i.

The far-IR spectra of $K[Hg(SCN)_3]$, $K_2[Hg(SCN)_4]$, and $Cs_2[Hg(SCN)_4]$ are shown in Figure 6. The spectrum of $K[Hg(SCN)_3]$ has two bands at 256 and 285 cm^{-1}, which are assigned to the symmetric and antisymmetric ν(HgS) modes, respectively. These bands occur in the Raman spectrum at 253 and 290 cm^{-1}, with their relative intensities reversed. These results compare with ν_s(HgS) = 270 (R) and ν_a(HgS) = 313 (IR) in solid $Hg(SCN)_2$.[58] The spectra of $K[Hg(SCN)_3]$ are consistent with the presence of $Hg(SCN)_2$ molecules with a nonlinear S−Hg−S structure, which results in both ν(HgS) modes being active in the IR and Raman spectra. However, the relatively high ν(HgS) values, and the fact that the relative band intensities approach those for a linear S−Hg−S structure, indicate that the interaction with the additional SCN^- ions in the solid is weak and that the S−Hg−S structure does not deviate much from linearity. This correlates well with the high $\Delta\sigma$ and low η values in the ^{199}Hg MAS NMR (Table 5), as discussed above. By contrast, the IR spectrum of $Cs[Hg(SCN)_3]$ shows three bands of comparable intensity at 263, 243, and 210 cm^{-1}. The lower wavenumbers of these bands relative to those of the potassium compound indicate a higher coordination number, but a trigonal planar HgS_3 coordination environment would give only one ν(HgS) band. The presence of three bands is a consequence of the distortion of the HgS_3 from ideal trigonal symmetry, and this correlates well with the lower $\Delta\sigma$ and higher η for this compound relative to the potassium salt (Table 5).

The IR spectrum of $K_2[Hg(SCN)_4]$ shows a single ν(HgS) band at 216 cm^{-1} (Figure 6). A single IR-active mode of T_2 symmetry is predicted for an ideal HgS_4 structure of T_d

(56) Davies, N. A.; Harris, R. K.; Olivieri, A. C. *Mol. Phys.* **1996**, *87*, 669.
(57) Barrie, P. J.; Clark, R. J. H.; Withnall, R.; Chung, D.-Y.; Kim, K.-W.; Kanatzidis, M. G. *Inorg. Chem.* **1994**, *33*, 1212.
(58) Cooney, R. P.; Hall, J. R. *Aust. J. Chem.* **1969**, *22*, 2117.

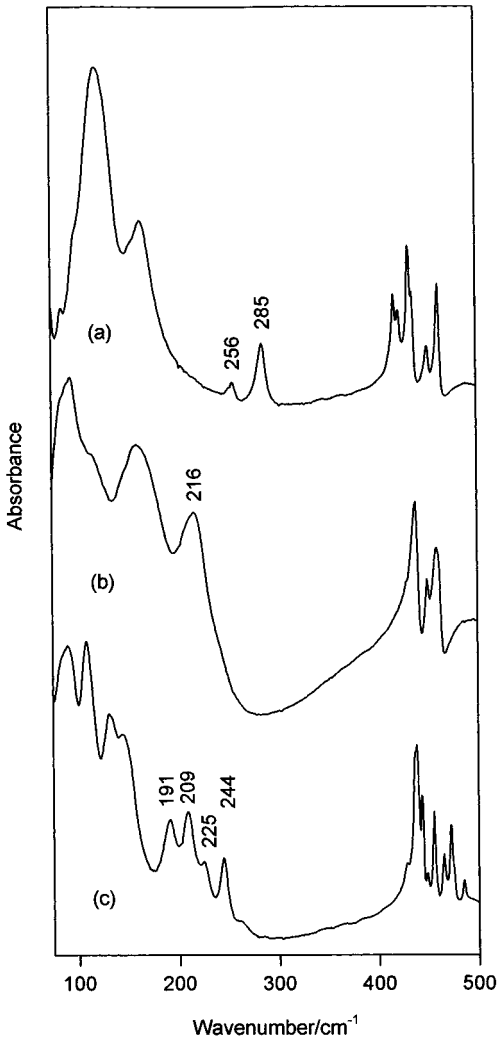

Figure 6. Far-IR spectra of (a) $K[Hg(SCN)_3]$, (b) $K_2[Hg(SCN)_4]$, and (c) $Cs_2[Hg(SCN)_4]$. Bands assigned to ν(HgS) are labeled with their wavenumbers.

symmetry. This correlates with the low $\Delta\sigma$ value for this complex (Table 5). By contrast, the IR spectrum of $Cs_2[Hg(SCN)_4]$ gives four ν(HgS) bands at 191, 209, 225, and 244 cm^{-1}. This indicates the presence of a distorted HgS_4 structure, which correlates well with the greater $\Delta\sigma$ value for this complex (Table 5). For a T_d HgS_4 structure, the symmetry and activity of the ν(HgS) modes are $A_1(R) + T_2(IR, R)$. For a nonaxially symmetric distortion, the A_1 mode becomes IR-active, and the triple degeneracy of the T_2 mode is completely lifted, so that a total of four IR bands is predicted, as observed. The nonaxial distortion correlates with the high η value from the NMR (Table 5); an axially symmetric distortion ($\eta = 0$) would result in activation of the A_1 mode and a splitting of the T_2 mode into a doublet, so that only three IR bands would result.

The above examples show how the solid-state NMR and vibrational spectra can provide complementary structural information.

The far-IR spectrum of $K_2[Hg_3(NCO)_8]$ shows a band at 425 cm^{-1}, while the Raman spectrum shows one at 358 cm^{-1}. These are assigned to the ν_a and ν_s Hg−N stretching modes, respectively, of the $Hg(NCO)_2$ units which this compound contains.[29] The corresponding vibrations in a properly characterized sample of $Hg(NCO)_2$ have not yet been reported. Other bands in the IR spectrum of $K_2[Hg_3(NCO)_8]$ are consistent with the presence of $Hg(NCO)_2$ molecules [2225, ν_a(NCO); 1319, ν_s(NCO); 601, δ(NCO) cm^{-1}] and NCO^- ions [2187, 2169, 2143, ν_a(NCO); 1299, ν_s(NCO); 655, 635, δ(NCO) cm^{-1}]. The resolution of separate bands due to bound and unbound NCO^- contrasts with the observation of only a single broad band in the ^{13}C MAS NMR spectrum (see above). The reason for this difference is not understood at present.

Acknowledgment. We thank C. Hobbis and J. Seakins for help with the vibrational spectroscopy, Se-Woung Oh for some preliminary MAS NMR measurements, and A. C. Olivieri for a copy of the error analysis routine for fitting spinning sideband manifolds.[37] G.A.B. thanks the University of Auckland for the award of a period of study leave. A.V.C. thanks The Royal Society and the University of Durham for financial support. We are grateful to the U.K. EPSRC for access to the Solid-State NMR Research Service based at the University of Durham.

Supporting Information Available: Tables listing detailed experimental data for X-ray diffraction, complete bond distances and bond angles, and anisotropic displacement parameters (6 pages). Ordering information is given on any current masthead page.

IC9700112